ACS OMEGA

http://pubs.acs.org/journal/acsodf

Article

Dual-Mode Multiple Ion Sensing via Analyte-Specific Modulation of Keto−Enol Tautomerization of an ESIPT Active Pyrene Derivative: Experimental Findings and Computational Rationalization

Suvendu Paul, Abhijnan Ray Choudhury, and Nilanjan Dey*

Cite This: *ACS Omega* 2023, 8, 6349−6360

Read Online

ACCESS | Metrics & More | Article Recommendations | Supporting Information

ABSTRACT: A pyrene-based *excited-state intramolecular proton transfer* (ESIPT) active probe **PMHMP** was synthesized, characterized, and employed for the ppb-level, dual-mode, and high-fidelity detection of Cu^{2+} (LOD: 7.8 ppb) and Zn^{2+} ions (LOD: 4.2 ppb) in acetonitrile medium. The colorless solution of **PMHMP** turned yellow upon the addition of Cu^{2+}, suggesting its ratiometric, naked-eye sensing. On the contrary, Zn^{2+} ions displayed concentration-dependent fluorescence rise till a 0.5 mole fraction and subsequent quenching. Mechanistic investigations indicated the formation of a 1:2 exciplex (Zn^{2+}:**PMHMP**) at a lower concentration of Zn^{2+}, which eventually turned into a more stable 1:1 (Zn^{2+}:**PMHMP**) complex with an additional amount of Zn^{2+} ions. However, in both cases, it was observed that the hydroxyl group and the nitrogen atom of the azomethine unit were involved in the metal ion coordination, which eventually altered the ESIPT emission. Furthermore, a green-fluorescent 2:1 **PMHMP**−Zn^{2+} complex was developed and additionally employed for the fluorimetric analysis of both Cu^{2+} and $H_2PO_4^-$ ions. The Cu^{2+} ion, owing to its higher binding affinity for **PMHMP**, could replace the Zn^{2+} ion from the preformed complex. On the other hand, $H_2PO_4^-$ formed a tertiary adduct with the Zn^{2+}−complex, leading to a distinguishable optical signal. Furthermore, extensive and organized density functional theory calculations were performed to explore the ESIPT behavior of **PMHMP** and the geometrical and electronic properties of the metal complexes.

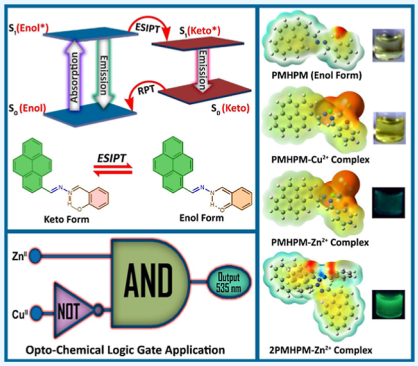

1. INTRODUCTION

Due to their significant role in physiochemical processes, selective recognition of transition metal ions particularly zinc and copper has become a focus of numerous studies in supramolecular chemistry. The Zn^{2+} ion, the second most abundant transition metal ion in the human body, plays essential roles in various cellular activities, such as regulation of gene expression, apoptosis, metalloenzyme catalysis, neurotransmission in biological systems, etc.[1] However, it has also been reported that the Zn^{2+} ion is a potent killer of neurons via oxidative stress.[2] Compared to other tissues, pancreatic islets contain relatively large concentrations of Zn^{2+}, which play a critical role in insulin biosynthesis, storage, and secretion.[3] A decrease in the concentration of Zn^{2+} can cause a reduction in the ability of the islet cells to produce and secrete insulin.[4] The Zn^{2+} ion does not give a spectroscopic or magnetic signal originating from its $3d^{10}4s^0$ electronic configuration; thus, the fluorescence method is a practical choice for detecting Zn^{2+}.[5] On the other hand, the soft transition metal ion Cu^{2+} is the third most abundant essential trace element in the human body. Various redox processes, enzyme functions, and pigments involve copper ions as their cofactors.[6] The World Health Organization (WHO) suggests that 10−12 mg per day must be the upper limit for copper consumption.[7] Free solvated copper ions can catalyze the formation of reactive organic species, including radical and non-radical species that participate in the initiation and/or propagation of radical chain reactions that can damage biomolecules.[8] Copper toxicity causes oxidative stress and related symptoms, leading to diabetes and neurodegenerative disorders such as Alzheimer's, Parkinson's, Menkes, and Wilson's diseases.[9] However, despite a considerable number of optical probes reported in the literature for simultaneous detection of both Zn^{2+} and Cu^{2+} ions,[10−25] there is still a demand for new colorimetric probes that can make distinguishable "naked-eye" detection in the visible-wavelength region. This is particularly fascinating as it does not involve sophisticated instruments or skilled technicians for execution.

At the same time, phosphates also play a vital role in chemistry and biology. Phosphates are the essential building blocks for nucleic acids and thus play an important role in protein and enzyme synthesis. Also, phosphates are necessary for bone and teeth formation.[26,27] Therefore, the development

Received: October 11, 2022
Accepted: January 11, 2023
Published: February 13, 2023

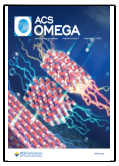

https://doi.org/10.1021/acsomega.2c06559
ACS Omega 2023, 8, 6349−6360

of selective receptors for phosphate anions and derivatives, such as $H_2PO_4^-$, pyrophosphate (PPi, $P_2O_7^{4-}$), adenosine triphosphate (ATP), adenosine diphosphate (ADP), *guanosine monophosphate*, adenosine monophosphate, and phosphoproteins, has reached the peak interest because of the vital roles that these chemical species play in a range of life processes.[28,29] In particular, fluorescent sensors are appealing as they allow for low-detection limit analysis and imaging.[30,31]

The excited-state intramolecular proton transfer (ESIPT) is one of the most popular photoprocesses in the field of colorimetric and fluorescent detection. The ESIPT behavior of the fluorophore **PMHMP** (Scheme 1) can be well presented in Figure 1.[32−34] Naturally, monitoring of the "on−off" switching between the tautomers of an ESIPT active probe and the detection and imaging of important cations, vital anions, and biological molecules have been achieved during the last 2 decades.[35−43] However, most surprisingly, there is almost no pyrene-based ESIPT active probe that has been utilized in the detection and imaging of analytes.[44] Unsurprisingly, the uniqueness and novelty of the present report are still significant in this sense. Moreover, a comparison table is designed assembling the ESIPT active probes that are involved in colorimetric and/or fluorescent detection of Cu^{2+} and Zn^{2+} ions. Table 1 displays two major concerns. The first one is the unavailability of an ESIPT active probe that can recognize both Cu^{2+} and Zn^{2+} ions in pure aqueous medium. There is no such ESIPT active pyrene derivative that is successful in dual-mode detection of Cu^{2+} and Zn^{2+} ions. Naturally, such variable concentration-dependent fluorescence behavior of the probe in the presence of Zn^{2+} is rare, interesting, and of high significance.

Scheme 1. Molecular Structure of PMHMP

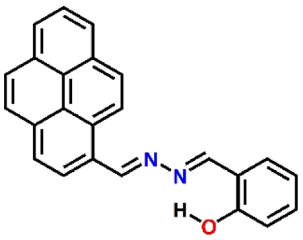

On the other hand, molecular logic gates are also one research focus of chemistry for further miniaturization in information technology. Various chemical systems have been developed to improvise different logic functions such as AND, OR, and NOT and their integrated operations.[45−47] Among them, those exhibiting more than one output channel with single molecules are currently of particular interest because they are the basis for constructing molecular logic circuits capable of executing special arithmetic operations and future security devices. In addition, many functional integrated logic gates such as INHIBIT, the half-subtractor, the half-adder, the full adder, and the full subtractor with various single molecules have been exploited.[48] Remembering these expediencies, **PMHMP** with a convenient logic function might be important in the field of the binary system and intelligent opto-chemical devices.

This report assembled the exploration of the ESIPT behavior of a pyrene-based amphiphilic probe (**PMHMP**) and dual-mode sensing of Cu^{2+} and Zn^{2+} ions along with $H_2PO_4^-$ and its opto-chemical application in the logic function. The addition of Cu^{2+} induced the formation of a yellow-colored solution and quenching of keto emission. On the other hand, at a lower concentration of Zn^{2+} ions, a bright-green fluorescence was observed due to exciplex formation. However, upon increasing the concentration further, we could observe the formation of a "thermodynamically stable" 1:1 complex with the Zn^{2+} ion with a relatively faint fluorescence signal. These results observed here can be used to construct an INHIBIT logic gate where both Cu^{2+} and Zn^{2+} ions will be involved as input signals. Furthermore, we prepared a highly fluorescent 1:2 Zn−**PMHMP** complex and employed the same for the fluorimetric detection of Cu^{2+} and $H_2PO_4^-$ ions. Furthermore, the ESIPT phenomenon and ion sensing mechanism of **PMHMP** were explored theoretically. To the best of our knowledge, there is practically no ESIPT active pyrene derivative probe in the existing literature which could be involved in the selective detection of Cu^{2+}, Zn^{2+}, and $H_2PO_4^-$ with such potential competency.

2. EXPERIMENTAL SECTION

2.1. Materials and Methods. All the chemicals, including the starting materials, cationic salts (Ag^+, Co^{2+}, Ca^{2+}, Cd^{2+}, Cu^{2+}, Hg^{2+}, Ni^{2+}, Pb^{2+}, Mg^{2+}, and Zn^{2+}), anionic tetrabuty-

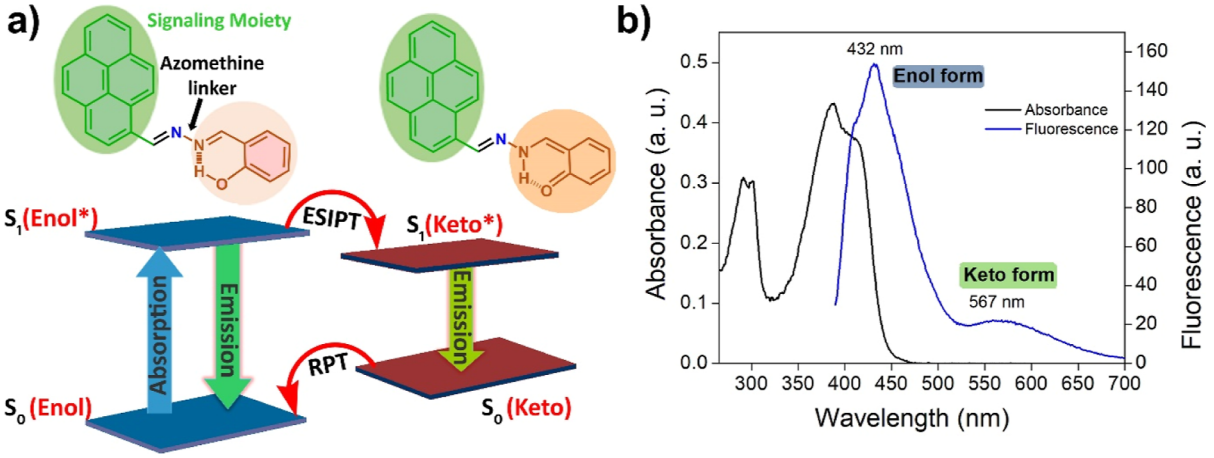

Figure 1. (a) Keto−enol tautomers of **PMHMP** along with the plausible ESIPT process. (b) UV−visible and fluorescence spectrum of **PMHMP** (10 μM, λ_{ex} = 350 nm) in acetonitrile medium.

https://doi.org/10.1021/acsomega.2c06559
ACS Omega 2023, 8, 6349−6360

Table 1. Comparison Table Containing the ESIPT Active Probes Involved in Colorimetric and/or Fluorescent Detection of Cu^{2+} and Zn^{2+} Including the Probe Structure, LOD of the Ions, Medium of Detection, and Fluorescence Response

Probe Structure	Ions detected	LOD of Cu^{2+}	LOD of Zn^{2+}	Fluorescence response	Solvent	Ref.
	Zn^{2+}	----	20 nM	Ratiometric	HEPES buffered $CH_3CN:H_2O$ (4:1; v/v), (pH= 7.0±0.1)	10
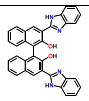	Cu^{2+} & Zn^{2+}	----	----	Turn off (Cu^{2+}); Ratiometric (Zn^{2+})		
	Cu^{2+}, Zn^{2+}, Cd^{2+}, $H_2PO_4^-$ and PPi	-----	650 nM	Turn on (Zn^{2+}/Cd^{2+}) followed by turn off ($H_2PO_4^-$ /PPi)	HEPES buffered MeOH:H_2O (pH= 7.3)	11
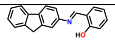	Cu^{2+}, Zn^{2+} and F^-	----	----	Turn on (Zn^{2+} and F^-)	HEPES buffered MeOH:H_2O (pH= 7.2)	12
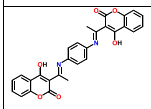	Cu^{2+} & Zn^{2+}	1.87 nM	19.4 nM	Turn off (Cu^{2+}); Turn on (Zn^{2+})	HEPES buffered $CH_3CN:H_2O$ (pH= 7.2)	13
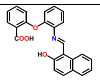	Cu^{2+} & Zn^{2+}	10 μM	10 μM	No significant change (Cu^{2+}), Turn on (Zn^{2+})	CH_3CN	14
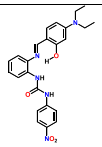	Cu^{2+} & Zn^{2+}	12.9 nM	----	Turn off (Cu^{2+}); Turn on (Zn^{2+})	CH_3CN	15
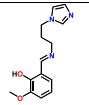	Cu^{2+} & Zn^{2+}	11.64 nM	31.04 nM	Turn on (Zn^{2+}) followed by Turn off (Cu^{2+})	HEPES buffered $CH_3CN:H_2O$ (pH= 7.2)	16
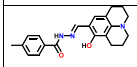	Cu^{2+} & Zn^{2+}	1.46 μM	35 nM	Turn on (Zn^{2+}) followed by turn off (Cu^{2+})	HEPES buffered $CH_3CN:H_2O$ (pH= 7.2)	17
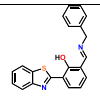	Cu^{2+} & Zn^{2+}	774 nM	911 nM	Turn off (Cu^{2+}) & turn on (Zn^{2+})	EtOH/HEPES (Zn^{2+}) & THF/HEPES (Cu^{2+}); pH= 7.4	18
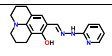	Co^{2+}, Ni^{2+}, Cu^{2+} & Zn^{2+}	623 nM	109 nM	Turn on (Zn^{2+})	EtOH/tris-HCl buffer (pH =7.4)	19
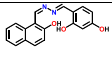	Co^{2+}, Cu^{2+} & Zn^{2+}	34.3 nM	37.0 nM	Turn on (Zn^{2+}) & no significant change for Cu^{2+}	HEPES buffered DMF:H_2O (pH= 7.0)	20
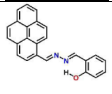	Cu^{2+}, Zn^{2+} & $H_2PO_4^-$	7.8 ppb	4.2 ppb	Colorimetric sensing of Cu^{2+} and fluorescence sensing of Zn^{2+}	CH_3CN	This work

lammonium (TBA^+X^-; X^- = F^-, Cl^-, Br^-, I^-, PF_6^-, ClO_4^-, AcO^-, CN^-, $H_2PO_4^-$, NO_3^-, N_3^-, and CO_3^{2-}) salts, solvents, and silica gel, were obtained from the reliable and reputed suppliers, like Sigma-Aldrich (Merck, Massachusetts, USA), Spectrochem (Spectrochem, Mumbai, India), etc., and used without further purification.

2.2. Methods. ^1H NMR and ^{13}C NMR spectra were recorded in dimethyl sulfoxide-d_6 (DMSO-d_6) using a Bruker Advance DRX 400 spectrometer operating at 400 and 100 MHz, respectively. Fourier-transform infrared (FT-IR) spectra were recorded using KBr pellets on a PerkinElmer FT-IR spectrum BX (PerkinElmer, Massachusetts, USA). The mass spectrum was recorded using a Micromass ESI-TOF MS instrument (Bruker, Massachusetts, USA). Elemental analysis was recorded using Thermo Finnigan EA FLASH 1112 SERIES (Thermo Finnigan, California, United States). The UV−visible absorption spectra were obtained on a UV-2100 spectrophotometer (Shimadzu, Osaka, Japan). Fluorescence spectra were recorded on a Fluorolog Horiba Jobin Yvon spectrofluorometer (Horiba, Kyoto, Japan). The stock solutions of the probe molecules were prepared in DMSO and diluted with acetonitrile before the spectroscopic studies. The slit width for the experiment was kept at 5 nm. Sensing was carried out by adding requisite amounts of cations to the acetonitrile solution of **PMHMP** (1×10^{-5} M).

2.3. Computational Details. All the quantum mechanical calculations of the neutral and cationic species were executed using the Gaussian 09W software package ignoring symmetrical constraints.[49] The ground (S_0) and first singlet excited state (S_1) calculations were performed with density functional theory (DFT) and time-dependent DFT (TD-DFT) methods, respectively, in combination with an M06-2X theoretical model and 6-311G basis set.[50,51] In the beginning, all the species were optimized in vacuum and then in acetonitrile (ε = 35.688), combining the integral equation formalism polarizable continuum model (IEFPCM).[52−55] For all the species, the global minima were confirmed by stability calculations and the IR spectral calculations with no imaginary frequency for S_0 and one for S_1. The potential energy scans of the ESIPT active probe were performed by altering one particular coordinate against the potential energy. The molecular electrostatic potential (MEP) 3D and highest occupied molecular orbital (HOMO)−lowest unoccupied molecular orbital (LUMO) images were extracted from the check-point files. For more insights into computational methods, authors might follow somewhere else.[56,57]

3. RESULTS AND DISCUSSION

3.1. Spectroscopic Studies. *3.1.1. UV−Visible Studies.* The fluorophore **PMHMP** was synthesized by following the procedure reported in the literature[44] and characterized accordingly (Scheme 1, Supporting Information). A weak peak characterizes the UV−vis spectrum of **PMHMP** in the 300 nm region, presumably caused by the n−π^* transition of the C═N group. Additionally, two prominent bands were observed in the 387 and 413 nm regions, which can be attributed to the $\pi-\pi^*$ transitions of phenyl and pyrene rings, respectively.[58] A distinct color change from colorless to yellow was observed immediately upon the addition of Cu^{2+} ions into the CH_3CN solution of **PMHMP**. No other metal ions, including Zn^{2+}, displayed any detectable color change even after incubating for a longer time. With the addition of Cu^{2+}, a red shift and broadening of the absorption band were

https://doi.org/10.1021/acsomega.2c06559
ACS Omega 2023, 8, 6349−6360

observed. As expected, no spectral change in the UV−visible study was observed upon the addition of Zn^{2+} ions. The titration studies with the Cu^{2+} ion showed a hyperchromic shift at 290 nm with the accompanying hypsochromic response at 387 and 412 nm bands. At the same time, a new band centered at 445 nm was formed upon titration with Cu^{2+}. Also, the two isosbestic points were observed at 360 and 424 nm during titration with Cu^{2+} ions, which indicated a one-to-one equilibrium between **PMHMP** and the corresponding Cu^{2+}−complex (Figure 2). When the ratios of absorbance at 290 and

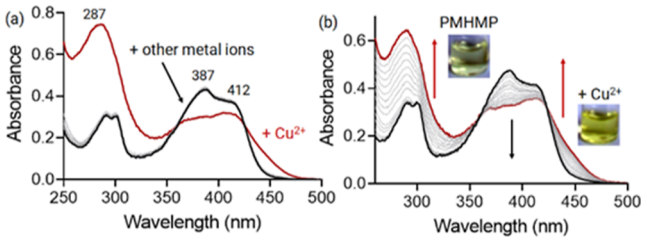

Figure 2. (a) UV−visible spectra of **PMHMP** (10 μM) with different metal ions (1.0 equiv) in acetonitrile medium. (b) UV−visible titration of **PMHMP** (10 μM) with Cu^{2+} ions (0−1.2 equiv) in acetonitrile medium.

388 nm bands were plotted against the equivalent of Cu^{2+} added, they appeared to be a straight line that established ratiometric, naked-eye sensing of Cu^{2+} (Figure S1, Supporting Information). The titration studies also indicated that the present system can detect Cu^{2+} ions as low as 7.8 ppb. Furthermore, the stoichiometry of the complex formed with Cu^{2+} was calculated using the method of continuous variation or Job's method.[59−62] The total molar concentration of Cu^{2+} and **PMHMP** was held constant, but their mole fractions varied. The changes in absorbance were plotted against the mole fractions of these two components, and from the maximum, on the plot, we could predict 1:1 stoichiometry with Cu^{2+} (Figure S2, Supporting Information). The association constant (log K) for the complex was calculated at 5.27 ± 0.025 using the Benesi−Hildebrand method for 1:1 stoichiometry.[63−65]

3.1.2. Fluorescence Studies. After a meaningful observation in the UV−vis study, we intended to perform a fluorescence study by exciting **PMHMP** at 350 nm in the CH_3CN medium. The fluorescence spectrum of **PMHMP** appeared to be broad and red-shifted (≈432 nm) with no pyrene-specific vibronic features. Due to the extended conjugated structure, this indicated more assertive electronic communication between pyrene and the iminophenol unit.[66] However, **PMHMP** exhibited faint-blue fluorescence (Φ = 0.04) under a long UV lamp, which might be due to the efficient photo-induced electron transfer (PET) attributed to the lone pair of electrons on the nitrogen atoms.[67] In addition, a broadband with relatively low intensity was observed in the 567 nm region, which might be due to emission from the keto tautomer.[44,68] To prove this, we recorded the fluorescence spectrum in the CH_3CN−water (1:1) mixture medium, which displayed a significant increase in emission intensity at 575 nm (Figure S3, Supporting Information). Thus, we can comment that the fluorescence maxima of **PMHMP** at 432 and 565 nm in the CH_3CN medium probably originated from the enol and keto tautomers, respectively, ascertaining the ESIPT phenomenon of **PMHMP**.

When Cu^{2+} was added to the acetonitrile solution of **PMHMP**, the emission intensity at 565 nm was quenched significantly, while the intensity at 432 nm remained primarily unaffected (Figure S4, Supporting Information). Thus, we could speculate that the prototropic equilibrium gets disrupted due to the involvement of the hydrazone and the adjacent hydroxyl group in coordination with Cu^{2+} ions. Also, the fluorescence turn-off response (Φ = 0.01) is partially attributed to the intramolecular charge transfer (ICT) process owing to Cu^{2+} coordination. Interestingly, the probe exhibited a selective fluorescence enhancement with Zn^{2+} with a maximum of 527 nm. Apart from Cu^{2+} and Zn^{2+} ions, no other metal ions induce any distinguishable change in the fluorescence signal.

It was observed that in the presence of Zn^{2+}, the fluorescence intensity was enhanced ≈16-fold (Figure 3).

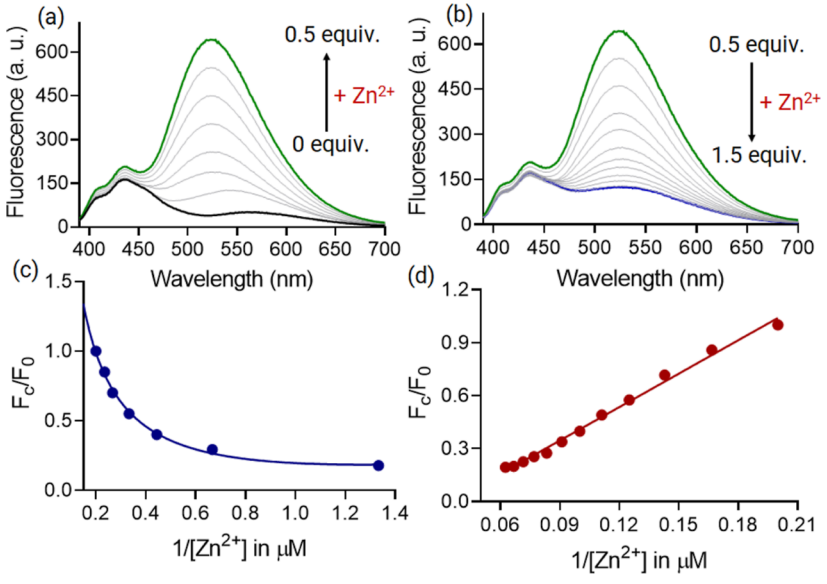

Figure 3. Fluorescence spectra of **PMHMP** (10 μM, λ_{ex} = 350 nm) with Zn^{2+} ions. (a) 0 to 0.5 and (b) 0.5−1.5 equiv in acetonitrile medium. Change in fluorescence intensity of **PMHMP** at 527 nm upon addition of Zn^{2+}. (c) 0 to 0.5 and (d) 0.5−1.5 equiv in acetonitrile medium.

https://doi.org/10.1021/acsomega.2c06559
ACS Omega 2023, 8, 6349−6360

The enhancement of fluorescence intensity (Φ = 0.14) with the addition of Zn^{2+} is probably due to the $\pi-\pi$ stacking of pyrene moieties and the formation of a static exciplex.[69] However, titration of the probe with Zn^{2+} in CH_3CN showed an interesting result. A substantial increase in the fluorescence intensity at the 527 nm band was witnessed until the $[Zn^{2+}]/[\mathbf{PMHMP}]$ mole ratio reached 0.5 (I/I_0 ratio is $\approx$ 16), followed by fluorescence quenching. We speculated that this abrupt change in the fluorescence signal during titration with Zn^{2+} ions might be due to a concentration-dependent change in the stoichiometry. At low concentrations, **PMHMP** probably formed a (1:2) complex with Zn^{2+} ions, while at the higher concentration (>0.5 equiv), it produced a (1:1) complex. Furthermore, we plotted F_c/F_0 as a function of varying $[Zn^{2+}]$, where F_c represent the fluorescence intensity for a specific concentration of added $[Zn^{2+}]$ and F_0 is the intensity of the free receptor. A non-linear variation of F_c/F_0 versus $1/[Zn^{2+}]$ at a lower concentration of Zn^{2+} ions confirmed a 1:2 complex formation. On the other hand, the linear F_c/F_0 versus $1/[Zn^{2+}]$ plot at a higher Zn^{2+} concentration suggested a 1:1 complexation.[70,71] The Job plot analysis with Zn^{2+} ions showed inflection points at mole fractions both 0.5 and 0.7 of **PMHMP**, indicating the presence of both 1:1 and 1:2 stoichiometric complexes with Zn^{2+} ions in the reaction medium (Figure S5, Supporting Information).

To increase the practical applicability of the sensing system, we checked the metal ion sensing ability of **PMHMP** in different water−acetonitrile mixtures. Although we could not see any response in the pure aqueous medium, Cu^{2+}-induced change in the absorption spectrum was witnessed in (9:1; v/v) acetonitrile−water mixture medium (very similar to what was observed in pure acetonitrile medium) (Figure S6, Supporting Information). Then, we performed UV−visible titration of **PMHMP** with Cu^{2+} under that condition, which similarly showed isosbestic points at 355 and 425 nm. Here also, we then plotted the ratio of absorbance at 288 and 388 nm with the equivalent of Cu^{2+} added; it appeared to be a straight line which established ratiometric sensing of Cu^{2+} (Figure S7, Supporting Information). However, no fluorescence enhancement was found after Zn^{2+} addition in the presence of the (9:1; v/v) acetonitrile−water mixture.

Furthermore, a synthetic reaction was carried out between $ZnCl_2$ and **PMHMP** (1:2) in a MeOH medium (at room temperature). The resultant $[Zn(\mathbf{PMHMP})_2Cl_2]$ complex was characterized by elemental analysis (Figure S8, Supporting Information). The mononuclear Zn complex exhibited a spectrum resembling the range obtained at a $[Zn^{2+}]/[L]$ mole ratio of 0.5 during titration studies (Figure 4). Titration

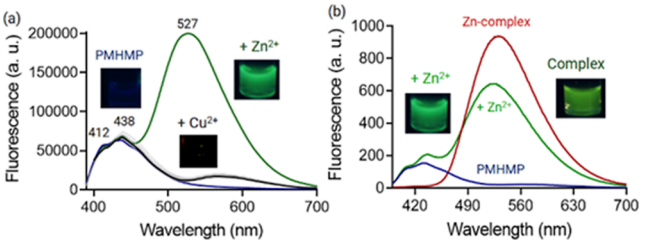

Figure 4. (a) Fluorescence spectra of **PMHMP** (10 μM, λ_{ex} = 350 nm) with different metal ions (0.5 equiv) in acetonitrile medium. (b) Fluorescence spectra of **PMHMP** (10 μM, λ_{ex} = 350 nm) with 0.5 equiv of Zn^{2+} and the preformed Zn−complex in acetonitrile medium.

of this complex with the Zn^{2+} ion showed a further quenching in fluorescence intensity, similar to what we observed during the titration studies (>0.5 equiv). The binding constant was calculated according to the Benassi−Hildebrand method and found to be (log K) 4.42 ± 0.031 (from the decreasing side of the titration curve, 1:1 stoichiometry) (Figure S9, Supporting Information). Fluorescence studies indicated that the present system can detect Zn^{2+} ions as low as 4.2 ppb in acetonitrile medium.

3.1.3. Mechanistic Investigations. We conducted spectroscopic studies to comment on the mode of interaction with Cu^{2+} and Zn^{2+} ions. The reversible binding of Cu^{2+} (Figure 5a) and/or Zn^{2+} (Figure S10, Supporting Information) ions was also checked using ethylenediaminetetraacetic acid (EDTA). The first metal ion at the requisite amount was added to the CH_3CN solution of **PMHMP**, and the same amount of EDTA was included. The addition of EDTA revived the original spectrum of **PMHMP**. This was repeated a few times, and we observed the revival of the original spectrum each time.

To comment on the binding mode, we performed the FT-IR studies of **PMHMP** with both Cu^{2+} (Figure S11, Supporting Information) and Zn^{2+} (Figure 5b) ions. Upon interaction with both Cu^{2+} and Zn^{2+} ions, the stretching frequency of the C═N band shifted to the lower-energy region, while the band corresponding to N−N shifted to the higher-energy region. On the other hand, in the FT-IR spectrum of the Zn complex, we found that the band at 1594 cm^{-1}, due to ($\nu_{C=N}$), shifted to 1539 cm^{-1} in the complex, suggesting coordination of the nitrogen atom of the azomethine group with the metal atom.[72] Due to (ν_{N-N}), the band shifts slightly from 1016 to 1021 cm^{-1} because it involves only one N atom of each azomethine unit in coordination. Furthermore, we performed ^1H NMR titration of **PMHMP** with Cu^{2+} and Zn^{2+} ions in DMSO-d_6 (Figure 5c). The NMR titration could not be performed in CD_3CN due to limited solubility.

All aromatic protons (belonging to pyrene and salicylaldehyde groups) experience chemical shifts upon the addition of Cu^{2+}. However, the extent of the shift was found to be more prominent for protons indicated as "a" and "b". Similarly, protons "c" and "d" were also affected as they were nearer to the azomethine and phenolic groups. This indicates that the coordination of Cu^{2+} occurred through phenolic oxygen and both N-atoms of the azomethine group. However, at a higher concentration of Cu^{2+}, there was a significant broadening of NMR signals. This must be due to the paramagnetic effect of Cu^{2+}, owing to its open-shell electronic configuration.[73] Interestingly, when titration was performed with Zn^{2+}, despite prominent chemical shifts at both pyrene and salicylaldehyde protons, no such broadening was observed. Such upfield shifts with Zn^{2+} ions indicate that pyrene and phenyl units are placed on top of each other in the metal complex.[74] To explain the concentration-dependent change in the stoichiometry of the in situ-formed Zn^{2+}−complex, we have recorded electrospray ionization-mass spectrometry mass spectra of **PMHMP** at different concentrations of added Zn^{2+} ions. At a mole fraction <0.5, we could observe the major peak at m/z 434, indicating the formation of the $[L_2{\cdot}Zn]^{2+}{\cdot}2H_2O$ complex (L = **PMHMP**). On the other hand, beyond 0.5 equiv, the peak at m/z 257 became more intense, which suggests 1:1 complexation $[\mathbf{L}{\cdot}Zn]^{2+}{\cdot}2H_2O$, with Zn^{2+} ions (Figure S12, Supporting Information).

3.1.4. Designing of the Logic Circuit. Molecular and supramolecular logic gates are candidates for computation at

https://doi.org/10.1021/acsomega.2c06559
ACS Omega 2023, 8, 6349−6360

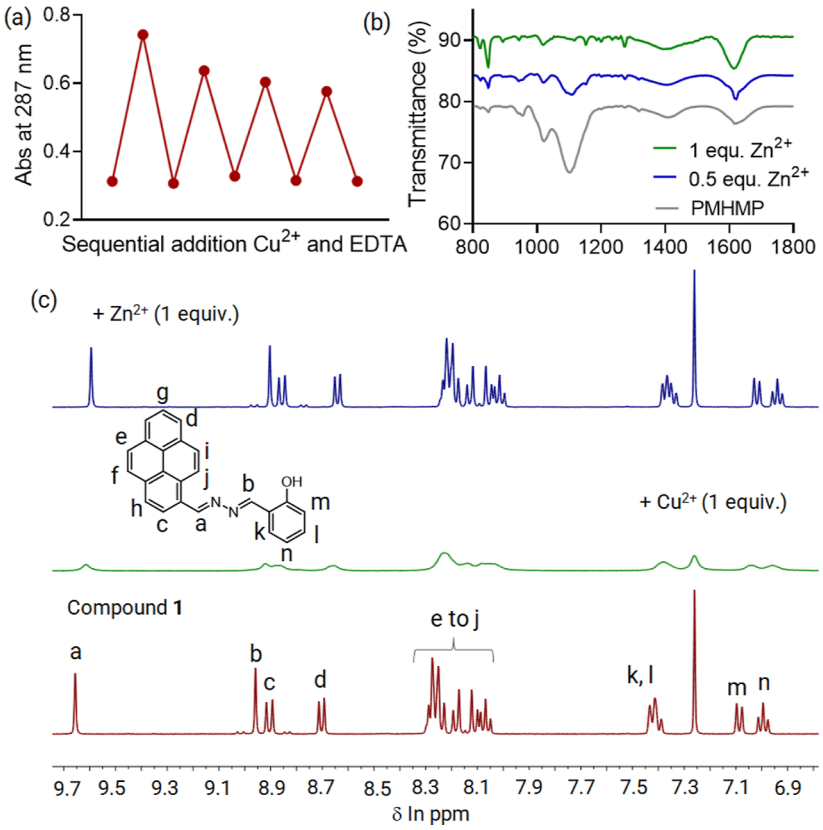

Figure 5. (a) Reversible interaction of **PMHMP** (10 μM) with Cu^{2+} ions (0.5 equiv) in acetonitrile medium. (b) FT-IR spectrum of **PMHMP** with Zn^{2+} ions (with 0.5 and 1 equiv). (c) ^{1}H NMR spectrum of **PMHMP** (5 mM) with Cu^{2+} and Zn^{2+} (1 equiv) in DMSO-d_6 medium.

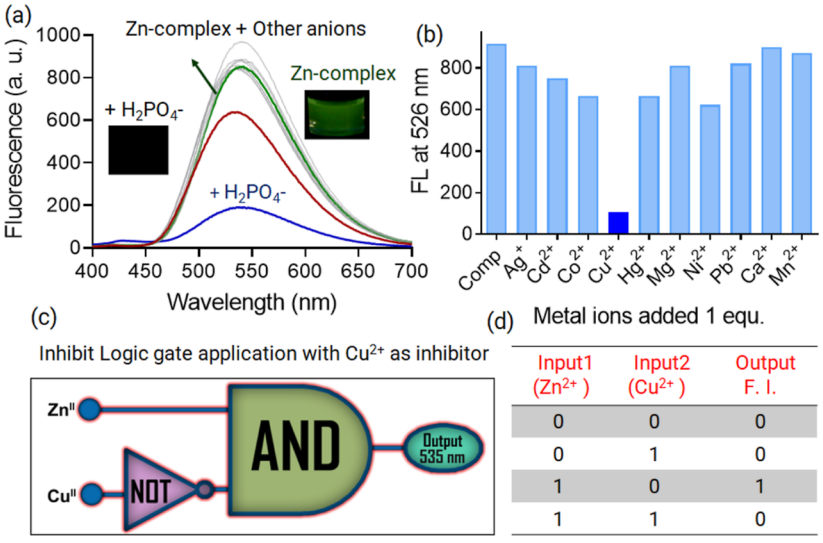

Input1 (Zn^{2+})	Input2 (Cu^{2+})	Output F. I.
0	0	0
0	1	0
1	0	1
1	1	0

Figure 6. (a) Fluorescence spectra of the Zn complex (10 μM, λ_{ex} = 350 nm) with anions (1 equiv) in acetonitrile medium. (b) Change in FL intensity of the Zn complex (10 μM, λ_{ex} = 350 nm) with metal ions (1 equiv) in acetonitrile medium. (c) Logic gate application of the Zn complex (10 μM, λ_{ex} = 350 nm) with Cu^{2+} and Zn^{2+} as inputs. (d) Truth table displayed the construction of the INHIBIT logic function.

the nano-scale level. Logic circuits, capable of performing arithmetic operations, have often been implemented in semiconductor technology. The optical signal of **PMHMP** could be affected distinctly by adding both Cu^{2+} and Zn^{2+} ions. Now, we have constructed binary logic functions with Zn^{2+} and Cu^{2+} as dual stimulating inputs and absorbance and fluorescence as outputs (Figure 6).[75,76]

Upon the addition of Zn^{2+} ions (Input-**1**), a new fluorescence band appeared at 527 nm, attributed to a typical exciplex formation as described above. On the contrary, in the presence of Cu^{2+} ions (Input-**2**), the emission band at 565 nm was quenched, probably due to the combined effect of PET and intramolecular charge transfer. However, when Cu^{2+} ions were added to the solution of **PMHMP**·Zn^{2+}, the quenching of fluorescence intensity at the 527 nm band was observed. Thus,

https://doi.org/10.1021/acsomega.2c06559
ACS Omega 2023, 8, 6349−6360

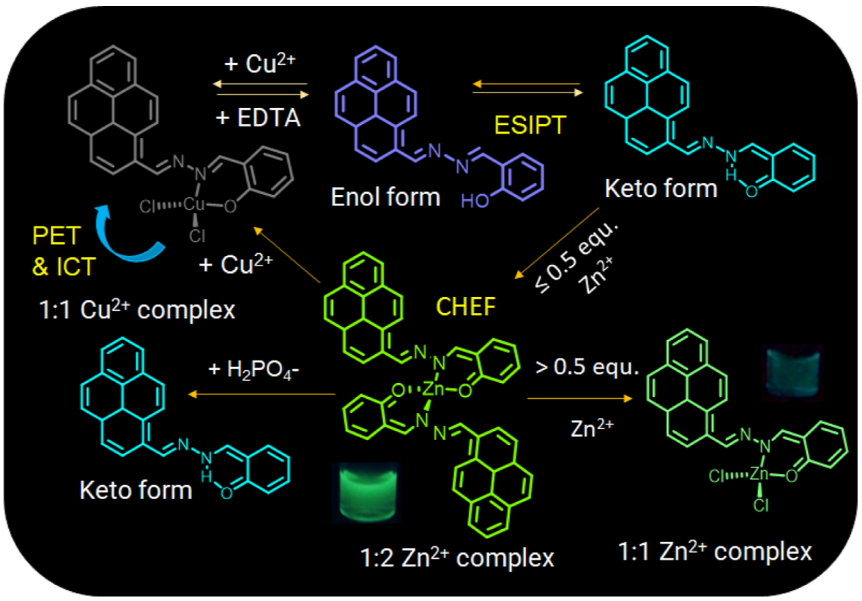

Figure 7. The schematic diagram shows stoichiometry dependence of **PMHMP** differential complexation modes for Cu^{2+} and Zn^{2+} ions.

we can presume that Cu^{2+} replaced the Zn^{2+} ion in the coordinated complex due to the higher binding ability of Cu^{2+} than that of Zn^{2+}. If we consider the relative fluorescence intensity (F_c/F_0, F_0 = fluorescence of **PMHMP** and F_c = **PMHMP** with metal ions) 14 as the threshold value, the output will be 0 when F_c/F_0 is lower than 14; output = 1 when the intensity is higher. Now, the fluorescence intensity is high enough only in the presence of Zn^{2+}, that is, only when IN1 = 1 and IN2 = 0; thus, under this condition, the output signal OUT = 1. Also, for all other cases when Cu^{2+} was present in the system, F_c/F_0 was lower than 14, so the outputs were 0. Therefore, it behaves like an INHIBIT logic gate, where Cu^{2+} ions act as an inhibitor.[77] This logic function demonstrates a non-communicative behavior in which one of the inputs can disable the whole system.

3.1.5. Sensing Applications with the Preformed Zn Complex. We have also checked the effects of different metal ions and anions upon the preformed Zn complex in the CH_3CN medium. Most of the metal ions (Ag^+, Co^{2+}, Ca^{2+}, Cd^{2+}, Cu^{2+}, Hg^{2+}, Ni^{2+}, Pb^{2+}, Mg^{2+}, and Zn^{2+}) showed little blue shifts ($\Delta\lambda \approx 7-8$ nm) in the emission maxima. However, with the addition of Cu^{2+} ions, along with a blue shift, we could also observe a large decrease (≈9-fold) in the fluorescence intensity. This observation indicated that Cu^{2+} ions, owing to their higher binding affinity for **PMHMP**, could replace Zn^{2+} ions from the complex.[78,79] We also observed a similar result when **PMHMP** was treated sequentially with Zn^{2+} and Cu^{2+} ions (Figures S13 and S14a, Supporting Information).

Furthermore, the preformed Zn^{2+} complex was exposed to a large number of anions (F^-, Cl^-, Br^-, I^-, PF_6^-, ClO_4^-, AcO^-, CN^-, $H_2PO_4^-$, SO_4^{2-}, NO_3^-, N_3^-, and CO_3^{2-}); only $H_2PO_4^-$ could selectively quench the intensity of the excimer band (≈18-fold). The other tested anions showed no interaction with the Zn complex. Then, we conducted fluorescence titration studies with $H_2PO_4^-$ ions under similar conditions, which showed a concentration-dependent linear quenching in emission intensity (Figure S14b, Supporting Information). The Job's plot analysis indicated a 1:1 complexation between the $H_2PO_4^-$ ion and Zn complex (Figure S15, Supporting Information). From the fluorescence titration studies, the association constant for $H_2PO_4^-$ was determined to be (log K) 6.14 ± 0.07. Along with quenching, $H_2PO_4^-$ ions also induced a small red shift ($\Delta\lambda \approx 8$ nm) in the emission maxima. This suggested that the coordination of the $H_2PO_4^-$ ion with the Zn^{2+} center probably perturbs the $\pi-\pi$ stacking interaction. The fluorescence spectrum in the presence of $H_2PO_4^-$ ions was found to be significantly different than that of free **PMHMP**. When Zn^{2+} ions were added to the $H_2PO_4^-$-treated solution of the Zn complex, the revival of the original fluorescence spectrum (of free **PMHMP**) was not observed (Figures 7 and S16, Supporting Information). Such observations indicated tertiary complex formation between the Zn complex and $H_2PO_4^-$ ions, where Zn^{2+} ions are simultaneously linked to **PMHMP** and $H_2PO_4^-$ ions.[80,81] The ^{31}P NMR spectrum of $H_2PO_4^-$ with the Zn complex showed a downfield shift in the signal (Figure S17a, Supporting Information). This further confirmed the binding of $H_2PO_4^-$ with the Zn^{2+} center. The ternary complex formation was also evident from mass spectral analysis, where we observed a new peak at m/z 855.1 (Figure S17b, Supporting Information). We also checked the interaction of the Zn complex with methyl phosphate, etc.[82,83] In this case, the extent of quenching was found to be substantially low (~2-fold) compared to $H_2PO_4^-$ ions (Figure S18, Supporting Information). This means that their extent of interaction was less effective as compared to $H_2PO_4^-$.

3.2. DFT Studies. *3.2.1. Optimized Geometry.* Since **PMHMP** contains two aromatic moieties (pyrene and benzene) which are connected by a rotatable azomethine moiety, we performed the potential energy scan study by keeping the pyrene moiety intact and rotating the benzene moiety along the dihedral axis, 27N−28N−29C−30C from −180 to +185° by varying 5° in each step to locate the minimum energy conformations (Figure S19, Supporting Information). From this figure, it was quite clear that **PMHMP** existed in three lower-energy conformations on its ground-state (S_0) potential energy surface with dihedral angles −180, 0, and +180°, and the transition energies for interconversion among the minimum energy conformations were quite high to achieve. Moreover, the conformations at the dihedral angles −180 and +180° equivalently denoted the enol

https://doi.org/10.1021/acsomega.2c06559
ACS Omega 2023, 8, 6349−6360

form of **PMHMP**. Among all the possible orientations, all three minimum energy geometries have the closest distance along the −N···H···O− axis. This result revealed that **PMHMP** exists in the enol form in S_0 and might show ESIPT phenomena to switch over into the keto form in the first singlet excited state (S_1) and is involved in intramolecular hydrogen bonding along the axis −N···H···O− in both keto and enol forms. Naturally, all the ground-state calculations were performed in the subsequent sections with the minimum energy conformation with the dihedral angle of +180°. Thereafter, **PMHMP** and its metal complexes (stoichiometry according to experimental observations) were optimized (Figure S20, Supporting Information). From the optimized geometry, it was observed that one N atom of **PMHMP** was in close proximity to −OH which might be involved in hydrogen bonding in S_0, but the other N atom with a lone pair might be involved in PET to the pyrene moiety. On the other hand, upon coordination of Cu^{2+} and Zn^{2+}, there was a flipping of the azomethine moiety of **PMHMP**. This might be a major reason behind the respective spectroscopic changes. On the flip side, in the $(\mathbf{PMHMP})_2$−Zn^{2+} complex, the probe reverted to its original conformation and displayed reverse spectral changes from the 1:1 Zn^{2+} complex.

3.2.2. MEP Studies. Since in this particular study, we focused on the ESIPT phenomena of **PMHMP** and its binding behavior with Cu^{2+} and Zn^{2+} ions and expecting significant charge reorganization, respective 3D MEP plots (isodensity value = 0.0004 a.u.) (Figure 8) were developed. The red-colored portion of the enol form of the probe denoted the electrophilic nature of the phenolic −OH and susceptibility of formation of an intramolecular hydrogen bond with the azomethine nitrogen and might be involved in ESIPT to transform into the keto form in the S_1 state. This type of conformation is a very common and natural behavior of the ESIPT active probes.[84] In both 1:1 Cu^{2+} and Zn^{2+}complexes, we observed a huge enhancement of electron density around the metal center including the benzene moiety. This indicated the possibility of ICT from the benzene to the pyrene moiety. However, for the Cu^{2+} complex, it occurred in the ground state, whereas for the Zn^{2+} complex, charge transfer occurred in the exciplex. Moreover, in the $(\mathbf{PMHMP})_2$−Zn^{2+} complex, the electron density over the benzene moieties was very low, whereas over pyrene moieties, it was quite high, denoting the inhibition of the charge transfer process.

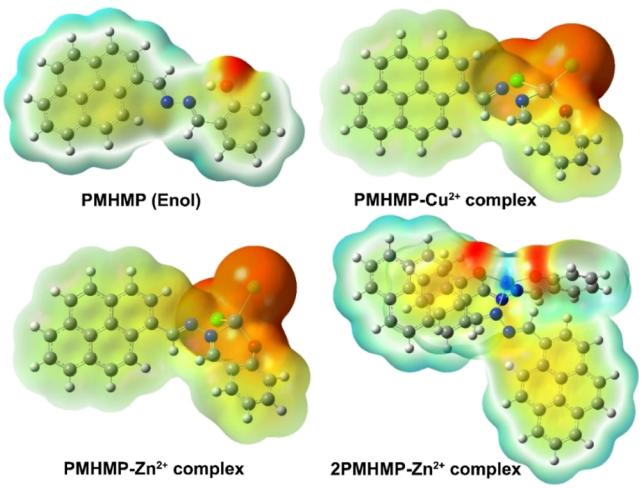

Figure 8. 3D MEP plots of **PMHMP** and its metal complexes in CH_3CN calculated using the DFT/M06-2X/6-311G theoretical model and IEFPCM solvent system.

3.2.3. Frontier Molecular Orbital Analysis. There is no need to mention that the change in electronic cloud distribution of frontier molecular orbitals (FMOs) particularly the HOMO and LUMO over a fluorophore evidently revealed its ESIPT probe.[84] The HOMO−LUMO images of both the enol and keto forms of **PMHMP** are presented in Figure S21, Supporting Information, and the Cu^{2+} and two Zn^{2+} complexes of **PMHMP** are presented in Figure 9. The electron density over the N atom of the enol form sharply increased from the HOMO to the LUMO. This charge transfer phenomenon strengthened the −N···H−O− intramolecular hydrogen bond strength and endorsed the proton transfer from oxygen to the nitrogen atom in the S_1 state. Moreover, there was a huge decrease in the HOMO−LUMO energy gap from the enol to the keto form which, in turn, supported the experimental observation (Figure 1a) and the ESIPT mechanism (Figure 1a). In addition, the computationally calculated UV−vis spectra of **PMHMP** displayed two absorption bands denoting the possibility of two tautomeric states of **PMHMP** (Figure S22, Supporting Information). In both the 1:1 Cu^{2+} and Zn^{2+} complexes of **PMHMP**, there was a decrease in the electron cloud over the benzene moiety from the HOMO to the LUMO, denoting the ICT process from the benzene to the pyrene moiety. However, in the 1:2 Zn^{2+}−**PMHMP** complex, we did not observe such transfer of the electron cloud but rather a high electron density over the pyrene moiety in both the HOMO and LUMO which indicated the inhibition of the charge transfer behavior in the exciplex.

3.2.4. Potential Energy Scan Studies. The potential energy scan study is a fantastic tool to describe and establish any ESIPT process very effortlessly.[85,86] Hence, to establish the ESIPT phenomenon of **PMHMP** conclusively, we performed the potential energy scan study along the ESIPT coordinate (N−H distance) of **PMHMP** for both S_0 and S_1 states as presented in Figure 10.

In S_0, the energy difference between the enol−keto forms was very high (4.58 kcal mol^{-1}) along with extremely high transition energy for the enol-to-keto conversion (5.92 kcal mol^{-1}) but low for the keto to enol transition (1.34 kcal mol^{-1}). Naturally, **PMHMP** exists majorly in the enol form in the ground state. On the reverse side, in S_1, the energy difference between the enol−keto forms was extremely low (0.16 kcal mol^{-1}) along with almost the same transition energy for the enol to keto conversion (3.05 kcal mol^{-1}) and the keto to enol transition (2.89 kcal mol^{-1}). Moreover, the keto form was slightly more stable than the enol form in S_1. Naturally, no other process could be observed other than the ESIPT process of **PMHMP**.

Based on the above-mentioned discussion, we could propose this plausible binding mechanism (Figure 7), which has already been argued throughout the article. **PMHMP** undergoes keto−enol tautomerism. 1:1 Cu^{2+} displayed ICT, and Zn^{2+} formed an exciplex with **PMHMP** in different stoichiometric ratios and different charge transfer behavior. Moreover, **PMHMP** was recovered from the metal complexes upon complexation with EDTA. All the events and photoprocesses are argued soundly with experimental shreds of evidence and theoretical justifications.

https://doi.org/10.1021/acsomega.2c06559
ACS Omega 2023, 8, 6349−6360

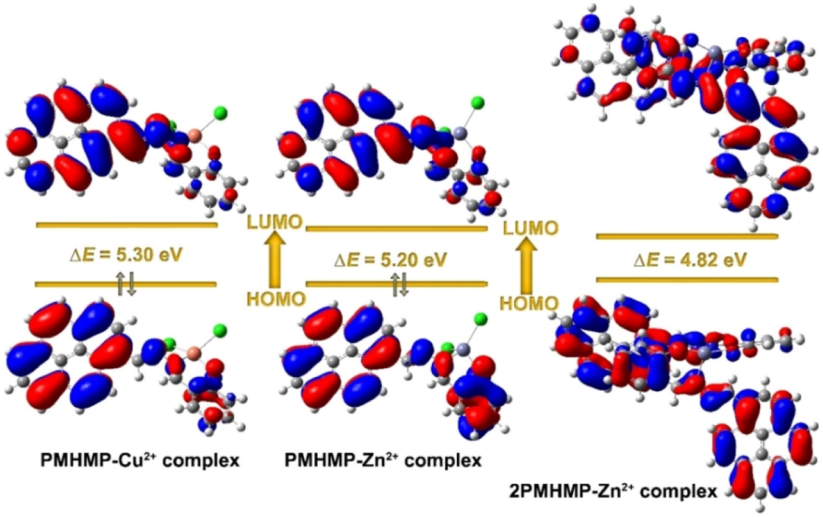

Figure 9. HOMO−LUMO images of Cu^{2+} and two Zn^{2+} complexes of **PMHMP** along with corresponding transition energy values calculated involving the DFT/M06-2X/6-311G theoretical model and CH_3CN/IEFPCM solvent system.

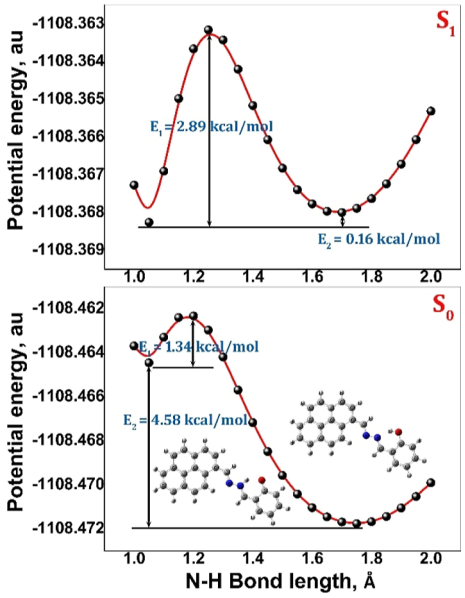

Figure 10. Potential energy scan plots along the ESIPT axis of **PMHMP** in S_0 (bottom) and S_1 (top) states calculated involving the DFT/M06-2X/6-311G theoretical model and CH_3CN/IEFPCM solvent system.

4. CONCLUSIONS

In conclusion, we have synthesized and characterized a pyrene-based probe (**PMHMP**), established its ESIPT behavior experimentally and theoretically, and employed it in dual-mode, ppb-level optical sensing of Cu^{2+} and Zn^{2+} ions. On the other hand, the keto emission of the compound was quenched upon the addition of Cu^{2+} ions. This indicated the inhibition of ESIPT emission upon coordination with metal ions. The probe can also be used as a "turn on" fluorescent sensor for Zn^{2+} ions. The exciplex formation was observed upon the addition of 0.5 equiv of Zn^{2+} ions. However, at a higher concentration of Zn^{2+} ions, we noticed the formation of a 1:1 complex with a faint fluorescence signal. Thus, we can detect and differentiate both Cu^{2+} and Zn^{2+} ions using UV−visible and fluorescence modes. Furthermore, the preformed 1:2 Zn^{2+}−**PMHMP** complex showed a "turn off" fluorescence response selectively in the presence of Cu^{2+} and $H_2PO_4^-$ ions. The Cu^{2+} ions, owing to higher binding affinity, could replace the Zn^{2+} ion, whereas $H_2PO_4^-$ ions could form a tertiary complex with the Zn complex. We have also constructed one INHIBIT logic function using Cu^{2+} and Zn^{2+} as the inputs in the emission mode. Therefore, pyrene derivative-based dual-mode, ppb-level detection of multiple ions with such unique behaviors is rare, interesting, and of high significance.

■ ASSOCIATED CONTENT

Supporting Information

The Supporting Information is available free of charge at https://pubs.acs.org/doi/10.1021/acsomega.2c06559.

Synthesis and characterization of the probe molecule and additional spectral and computational data (PDF)

■ AUTHOR INFORMATION

Corresponding Author

Nilanjan Dey − *Department of Chemistry, BITS-Pilani Hyderabad Campus, Hyderabad, Telangana 500078, India;* orcid.org/0000-0002-3988-1509; Email: nilanjandey.iisc@gmail.com

Authors

Suvendu Paul − *Department of Chemistry, BITS-Pilani Hyderabad Campus, Hyderabad, Telangana 500078, India;* orcid.org/0000-0001-9544-0102

Abhijnan Ray Choudhury − *Syngene International Limited, Hyderabad, Telangana 500078, India*

Complete contact information is available at: https://pubs.acs.org/10.1021/acsomega.2c06559

Notes

The authors declare no competing financial interest.

■ ACKNOWLEDGMENTS

The authors acknowledge BITS Pilani, Hyderabad, for central analytical facilities. ND thanks the SERB-SRG grant (SRG/2022/000031) for funding and technical support.

REFERENCES

(1) Xu, Z.; Yoon, J.; Spring, D. R. Fluorescent Chemosensors for Zn^{2+}. *Chem. Soc. Rev.* **2010**, *39*, 1996−2006.
(2) Sayre, L. M.; Perry, G.; Smith, M. A. Oxidative Stress and Neurotoxicity. *Chem. Res. Toxicol.* **2008**, *21*, 172−188.
(3) Fu, Z.; Gilbert, E. R.; Liu, D. Regulation of Insulin Synthesis and Secretion and Pancreatic Beta-cell Dysfunction in Diabetes. *Curr. Diabetes Rev.* **2013**, *9*, 25−53.
(4) Ohta, S.; Ikemoto, T.; Wada, Y.; Saito, Y.; Yamada, S.; Imura, S.; Morine, Y.; Shimada, M. A Change in the Zinc Ion Concentration Reflects the Maturation of Insulin-Producing Cells Generated from Adipose-Derived Mesenchymal Stem Cells. *Sci. Rep.* **2019**, *9*, 18731.
(5) Wang, F.; Wang, K.; Kong, Q.; Wang, J.; Xi, D.; Gu, B.; Lu, S.; Wei, T.; Chen, X. Recent Studies Focusing on the Development of Fluorescence Probes for Zinc Ion. *Coord. Chem. Rev.* **2021**, *429*, 213636.
(6) Liu, S.; Wang, Y. -M.; Han, J. Fluorescent Chemosensors for Copper(II) Ion: Structure, Mechanism and Application. *J. Photochem. Photobiol., C* **2017**, *32*, 78−103.
(7) Taylor, A. A.; Tsuji, J. S.; Garry, M. R.; McArdle, M. E.; Goodfellow, W. L., Jr.; Adams, W. J.; Menzie, C. A. Critical Review of Exposure and Effects: Implications for Setting Regulatory Health Criteria for Ingested Copper. *Environ. Manag.* **2020**, *65*, 131−159.
(8) Basa, P. N.; Sykes, A. G. Differential Sensing of Zn(II) and Cu(II) via Two Independent Mechanisms. *J. Org. Chem.* **2012**, *77*, 8428−8434.
(9) Gaetke, L. M.; Chow, C. K. Copper Toxicity, Oxidative Stress, and Antioxidant Nutrients. *Toxicology* **2003**, *189*, 147−163.
(10) Luxami, V.; Kumar, S. ESIPT based Dual Fluorescent Sensor and Concentration Dependent Reconfigurable Boolean Operators. *RSC Adv.* **2012**, *2*, 8734−8740.
(11) Gogoi, A.; Samanta, S.; Das, G. A Benzothiazole Containing CHEF Based Fluorescence Turn-ON Sensor for Zn^{2+} and Cd^{2+} and Subsequent Sensing of $H_2PO_4^-$ and $P_4O_7^{4-}$ in Physiological pH. *Sens. Actuators, B* **2014**, *202*, 788−794.
(12) Hens, A.; Rajak, K. K. Selective Fluorometric Detection of F^- and Zn(II) Ions by a N,O Coordinating Sensor and Naked Eye Detection of Cu(II) Ions in Mixed-Aqueous Solution. *RSC Adv.* **2015**, *5*, 44764−44777.
(13) Sarkar, D.; Pramanik, A. K.; Mondal, T. K. A Novel Coumarin based Molecular Switch for Dual Sensing of Zn(II) and Cu(II). *RSC Adv.* **2015**, *5*, 7647−7653.
(14) Kundu, A.; Hariharan, P. S.; Prabakaran, K.; Anthony, S. P. Synthesis of New Colori/Fluorimetric Chemosensor for Selective Sensing of Biologically Important Fe^{3+}, Cu^{2+} and Zn^{2+} Metal Ions. *Spectrochim. Acta, Part A* **2015**, *151*, 426−431.
(15) Singh, H.; Bhargava, G.; Kumar, S.; Singh, P. Quadruple-Signaling (PET, ICT, ESIPT, -C=N- rotation) Mechanism-based Dual Chemosensor for Detection of Cu^{2+} and Zn^{2+} ions: TRANSFER, INH and Complimentary OR/NOR Logic Circuits. *J. Photochem. Photobiol. A* **2018**, *357*, 175−184.
(16) Ansari, S. N.; Saini, A. K.; Kumari, P.; Mobin, S. M. An Imidazole Derivative-based Chemodosimeter for Zn^{2+} and Cu^{2+} Ions through "ON-OFF-ON" Switching with Intracellular Zn^{2+} Detection. *Inorg. Chem. Front.* **2019**, *6*, 736−745.
(17) Ganesan, J. S.; Gandhi, S.; Radhakrishnan, K.; Balasubramaniem, A.; Sepperumal, M.; Ayyanar, S. Execution of Julolidine based Derivative as Bifunctional Chemosensor for Zn^{2+} and Cu^{2+} Ions: Applications in Bio-Imaging and Molecular Logic Gate. *Spectrochim. Acta, Part A* **2019**, *219*, 33−43.
(18) Zheng, H.-W.; Kang, Y.; Wu, M.; Liang, Q.-F.; Zheng, J.-Q.; Zheng, X.-J.; Jin, L.-P. ESIPT-AIE active Schiff base based on 2-(2′-hydroxyphenyl)benzo-thiazole applied as multi-functional fluorescent chemosensors. *Dalton Trans.* **2021**, *50*, 3916−3922.
(19) Liu, H.; Ding, S.; Lu, Q.; Jian, Y.; Wei, G.; Yuan, Z. A Versatile Schiff Base Chemosensor for the Determination of Trace Co^{2+}, Ni^{2+}, Cu^{2+}, and Zn^{2+} in the Water and Its Bioimaging Applications. *ACS Omega* **2022**, *7*, 7585−7594.
(20) Yadav, P.; Gond, S.; Shekher, A.; Gupta, S. C.; Singh, U. P.; Singh, V. P. A Multifunctional Basic pH Indicator Probe for Distinguishable Detection of Co^{2+}, Cu^{2+} and Zn^{2+} with Its Utility in Mitotracking and Monitoring Cytoplasmic Viscosity in Apoptotic Cells. *Dalton Trans.* **2022**, *51*, 6927−6935.
(21) Wu, X.; Shi, W.; Yang, Y.; Zhao, D.; Li, Y. Multi-targeted Fluorescent Probes for Detection of Zn(II) and Cu(II) Ions based on ESIPT Mechanism. *Spectrochim. Acta Part A* **2023**, *287*, 122051.
(22) Jiménez-Sánchez, A.; Ortiz, B.; Navarrete, V. O.; Flores, J. C.; Farfán, N.; Santillan, R. A Dual-Model Fluorescent Zn^{2+}/Cu^{2+} Ions Sensor with *in-situ* Detection of $S^{2-}/(PO_4)^-$ and Colorimetric Detection of Fe^{2+} Ion. *Inorg. Chim. Acta* **2015**, *429*, 243−251.
(23) Anbu, S.; Ravishankaran, R.; Guedes da Silva, M. F. C. G. D.; Karande, A. A.; Pombeiro, A. J. L. Differentially Selective Chemosensor with Fluorescence Off−On Responses on Cu^{2+} and Zn^{2+} Ions in Aqueous Media and Applications in Pyrophosphate Sensing, Live Cell Imaging, and Cytotoxicity. *Inorg. Chem.* **2014**, *53*, 6655−6664.
(24) Mandal, J.; Ghorai, P.; Pal, K.; Karmakar, P.; Saha, A. 2-hydroxy-5-methylisophthalaldehyde based Fluorescent-Colorimetric Chemosensor for Dual Detection of Zn^{2+} and Cu^{2+} with High Sensitivity and Application in Live Cell Imaging. *J. Lumin.* **2019**, *205*, 14−22.
(25) Sakunkaewkasem, S.; Petdum, A.; Panchan, W.; Sirirak, J.; Charoenpanich, A.; Sooksimuang, T.; Wanichacheva, N. Dual-Analyte Fluorescent Sensor based on [5]helicene Derivative with Super Large Stokes Shift for the Selective Determinations of Cu^{2+} or Zn^{2+} in Buffer Solutions and Its Application in a Living Cell. *ACS Sens.* **2018**, *3*, 1016−1023.
(26) Yuan, Y. -X.; Wang, J. -H.; Zheng, Y. -S. Selective Fluorescence Turn-On Sensing of Phosphate Anion in Water by Tetraphenylethylene Dimethylformamidine. *Chem.−Asian J.* **2019**, *14*, 760−764.
(27) Law al, A. T.; Adeloju, S. B. Progress and Recent Advances in Phosphate Sensors: A Review. *Talanta* **2013**, *114*, 191−203.
(28) Zhou, Y.; Xu, Z.; Yoon, J. Fluorescent and Colorimetric Chemosensors for Detection of Nucleotides, FAD and NADH: Highlighted Research During 2004-2010. *Chem. Soc. Rev.* **2011**, *40*, 2222−2235.
(29) Gulyani, A.; Dey, N.; Bhattacharya, S. A Unique Self-Assembly-Driven Probe for Sensing a Lipid Bilayer: Ratiometric Probing of Vesicle to Micelle Transition. *Chem. Commun.* **2018**, *54*, 5122−5125.
(30) Kan, J.; Zhou, X.; Sun, Y.; Sun, L.; Chu, H.; Qian, Z.; Zhou, J. Molecular Engineering and Biomedical Applications of Ultra-Sensitive Fluorescent Probe for Ag^+. *Chin. Chem. Lett.* **2021**, *32*, 3066−3070.
(31) Liu, Z.; Zheng, Y.; Xie, T.; Chen, Z.; Huang, Z.; Ye, Z.; Xiao, Y. Clickable Rhodamine Spirolactam Based Spontaneously Blinking Probe for Super-Resolution Imaging. *Chin. Chem. Lett.* **2021**, *32*, 3862−3864.
(32) Chen, C. -L.; Chen, Y. -T.; Demchenko, A. P.; Chou, P. -T. Amino Proton Donors in Excited-State Intramolecular Proton-Transfer Reactions. *Nat. Rev. Chem.* **2018**, *2*, 131−143.
(33) Padalkar, V. S.; Seki, S. Excited-State Intramolecular Proton-Transfer (ESIPT)-Inspired Solid State Emitters. *Chem. Soc. Rev.* **2016**, *45*, 169−202.
(34) Paul, B. K.; Ganguly, A.; Guchhait, N. Quantum Chemical Exploration of the Intramolecular Hydrogen Bond Interaction in 2-thiazol-2-yl-phenol and 2-benzothiazol-2-yl-phenol in the Context of Excited-State Intramolecular Proton Transfer: A Focus on the Covalency in Hydrogen Bond. *Spectrochim. Acta, Part A* **2014**, *131*, 72−81.
(35) Sedgwick, A. C.; Wu, L.; Han, H. -H.; Bull, S. D.; He, X. -P.; James, T. D.; Sessler, J. L.; Tang, B. Z.; Tian, H.; Yoon, J. Excited-State Intramolecular Proton-Transfer (ESIPT) based Fluorescence Sensors and Imaging Agents. *Chem. Soc. Rev.* **2018**, *47*, 8842−8880.
(36) Odyniec, M. L.; Park, S. -J.; Gardiner, J. E.; Webb, E. C.; Sedgwick, A. C.; Yoon, J.; Bull, S. D.; Kim, H. M.; James, T. D. A Fluorescent ESIPT-based Benzimidazole Platform for the Ratiometric Two-Photon Imaging of $ONOO^-$ *in vitro* and *ex vivo*. *Chem. Sci.* **2020**, *11*, 7329−7334.

https://doi.org/10.1021/acsomega.2c06559
ACS Omega 2023, 8, 6349−6360

(37) Hu, R.; Feng, J.; Hu, D.; Wang, S.; Li, S.; Li, Y.; Yang, G. A Rapid Aqueous Fluoride Ion Sensor with Dual Output Modes. *Angew. Chem. Int. Ed.* **2010**, *49*, 4915−4918.
(38) Paul, S.; Karar, M.; Das, B.; Mallick, A.; Majumdar, T. Theory after Experiment on Sensing Mechanism of a Newly Developed Sensor Molecule: Converging or Diverging? *Chem. Phys. Lett.* **2017**, *689*, 199−205.
(39) Paul, S.; Majumdar, T.; Mallick, A. Hydrogen Bond Regulated Hydrogen Sulfate ion Recognition: An Overview. *Dalton Trans.* **2021**, *50*, 1531−1549.
(40) Chen, Y.; Fang, Y.; Gu, H.; Qiang, J.; Li, H.; Fan, J.; Cao, J.; Wang, F.; Lu, S.; Chen, X. Color-Tunable and ESIPT-Inspired Solid Fluorophores Based on Benzothiazole Derivatives: Aggregation-Induced Emission, Strong Solvatochromic Effect, and White Light Emission. *ACS Appl. Mater. Interfaces* **2020**, *12*, 55094−55106.
(41) Kong, Q.; Wang, J.; Chen, Y.; Zheng, S.; Chen, X.; Wang, Y.; Wang, F. The Visualized Fluorescent Probes Based on Benzothiazole Used to Detect Esterase. *Dyes Pigm.* **2021**, *191*, 109349.
(42) Zheng, S.; Fang, Y.; Chen, Y.; Kong, Q.; Wang, F.; Chen, X. Benzothiazole Derivatives based Colorimetric and Fluorescent Probes for Detection of Amine/Ammonia and Monitoring the Decomposition of Urea by Urease. *Spectrochim. Acta, Part A* **2022**, *267*, 120616.
(43) Pei, X.; Fang, Y. H.; Gu, H.; Zheng, S.; Bin, X.; Wang, F.; He, M.; Lu, S.; Chen, X. A Turn-On Fluorescent Probe Based on ESIPT and AIEE Mechanisms for the Detection of Butyrylcholinesterase Activity in Living Cells and in Non-Alcoholic Fatty Liver of Zebrafish. *Spectrochim. Acta, Part A* **2023**, *287*, 122044.
(44) Zang, L.; Jiang, S. Substituent Effects on Anion Sensing of Salicylidene Schiff Base Derivatives: Tuning Sensitivity and Selectivity. *Spectrochim. Acta, Part A* **2015**, *150*, 814−820.
(45) de Silva, A. P.; Gunaratne, H. Q. N.; McCoy, C. P. A Molecular Photoionic AND Gate based on Fluorescent Signalling. *Nature* **1993**, *364*, 42−44.
(46) Liu, L.; Liu, P.; Ga, L.; Ai, J. Advances in Applications of Molecular Logic Gates. *ACS Omega* **2021**, *6*, 30189−30204.
(47) Karar, M.; Paul, P.; Paul, S.; Haldar, B.; Mallick, A.; Majumdar, T. Dual Macro-Cyclic Component based Logic Diversity. *Dyes Pigm.* **2020**, *174*, 108060.
(48) Erbas-Cakmak, S.; Kolemen, S.; Sedgwick, A. C.; Gunnlaugsson, T.; James, T. D.; Yoon, J.; Akkaya, E. U. Molecular Logic Gates: The Past, Present and Future. *Chem. Soc. Rev.* **2018**, *47*, 2228−2248.
(49) Frisch, M. J.; Trucks, G. W.; Schlegel, H. B.; Scuseria, G. E.; Robb, M. A.; Cheeseman, J. R.; Scalmani, G.; Barone, V.; Mennucci, B.; Petersson, G. A.; Nakatsuji, H.; Caricato, M.; Li, X.; Hratchian, H. P.; Izmaylov, A. F.; Bloino, J.; Zheng, G.; Sonnenberg, J. L.; Hada, M.; Ehara, M.; Toyota, K.; Fukuda, R.; Hasegawa, J.; Ishida, M.; Nakajima, T.; Honda, Y.; Kitao, O.; Nakai, H.; Vreven, T.; Montgomery, J. A.; Peralta, J. E., Jr.; Ogliaro, F.; Bearpark, M.; Heyd, J. J.; Brothers, E.; Kudin, K. N.; Staroverov, V. N.; Kobayashi, R.; Normand, J.; Raghavachari, K.; Rendell, A.; Burant, J. C.; Iyengar, S. S.; Tomasi, J.; Cossi, M.; Rega, N.; Millam, J. M.; Klene, M.; Knox, J. E.; Cross, J. B.; Bakken, V.; Adamo, C.; Jaramillo, J.; Gomperts, R.; Stratmann, R. E.; Yazyev, O.; Austin, A. J.; Cammi, R.; Pomelli, C.; Ochterski, J. W.; Martin, R. L.; Morokuma, K.; Zakrzewski, V. G.; Voth, G. A.; Salvador, P.; Dannenberg, J. J.; Dapprich, S.; Daniels, A. D.; Farkas, O.; Foresman, J. B.; Ortiz, J. V.; Cioslowski, J.; Fox, D. J. *Gaussian 09*, Revision A.02; Gaussian, Inc.: Wallingford, CT, 2009.
(50) Zhao, Y.; Truhlar, D. G. The M06 Suite of Density Functionals for Main Group Thermochemistry, Thermochemical Kinetics, Noncovalent Interactions, Excited States, and Transition Elements: Two New Functionals and Systematic Testing of Four M06-Class Functionals and 12 Other Functionals. *Theor. Chem. Acc.* **2008**, *120*, 215−241.
(51) Zhao, Y.; Truhlar, D. G. A New Local Density Functional for Main-Group Thermochemistry, Transition Metal Bonding, Thermochemical Kinetics, and Noncovalent Interactions. *J. Chem. Phys.* **2006**, *125*, 194101−194118.
(52) Mennucci, B.; Cancès, E.; Tomasi, J. Evaluation of Solvent Effects in Isotropic and Anisotropic Dielectrics and in Ionic Solutions with a Unified Integral Equation Method: Theoretical Bases, Computational Implementation, and Numerical Applications. *J. Phys. Chem. B* **1997**, *101*, 10506−10517.
(53) Cancès, E.; Mennucci, B.; Tomasi, J. A New Integral Equation Formalism for the Polarizable Continuum Model: Theoretical Background and Applications to Isotropic and Anisotropic Dielectrics. *J. Chem. Phys.* **1997**, *107*, 3032−3041.
(54) Cammi, R.; Tomasi, J. Remarks on the Use of the Apparent Surface Charges (ASC) Methods in Solvation Problems: Iterative Versus Matrix-Inversion Procedures and the Renormalization of the Apparent Charges. *J. Comput. Chem.* **1995**, *16*, 1449−1458.
(55) Miertus, S.; Scrocco, E.; Tomasi, J. Electrostatic Interaction of a Solute with a Continuum. A Direct Utilizaion of AB Initio Molecular Potentials for the Prevision of Solvent Effects. *Chem. Phys.* **1981**, *55*, 117−129.
(56) Paul, S.; Mallick, A.; Majumdar, T. Computational Study on the Ion Interaction of Ellipticine: A Theoretical Approach toward Selecting the Appropriate Anion. *Chem. Phys. Lett.* **2015**, *634*, 29−36.
(57) Paul, S.; Karar, M.; Mitra, S.; Sher Shah, S. A.; Majumdar, T.; Mallick, A. A Molecular Lock with Hydrogen Sulfate as "Key" and Fluoride as "Hand": Computing Based Insights on the Functioning Mechanism. *ChemistrySelect* **2016**, *1*, 5547−5553.
(58) Zainuri, D. A.; Abdullah, M.; Zaini, M. F.; Bakhtiar, H.; Arshad, S.; Abdul Razak, I. A. Fused Ring Effect on Optical Nonlinearity and Structure Property Relationship of Anthracenyl Chalcone based Push-Pull Chromophores. *PLoS One* **2021**, *16*, No. e0257808.
(59) Fernandes, R. S.; Dey, N. Acyl Hydrazone-based Reversible Optical Switch for Reporting of Cyanide Ion in Industrial Wastewater Samples. *J. Mol. Struct.* **2022**, *1262*, 132968.
(60) Fernandes, R. S.; Dey, N. Anion Binding Studies with Anthraimidazoledione-based Positional Isomers: A Comprehensive Analysis of Different Strategies for Improved Selectivity. *Talanta* **2022**, *250*, 123703.
(61) Paul, S.; Fernandes, R. S.; Dey, N. Ppb-level, Dual Channel Sensing of Cyanide and Bisulfate Ions in an Aqueous Medium: Computational Rationalization of the Ion-Dependent ICT Mechanism. *New J. Chem.* **2022**, *46*, 18973−18983.
(62) Chettri, B.; Jha, S.; Dey, N. Unique CT Emission from Aryl Terpyridine Nanoparticles in Aqueous Medium: A Combined Effect of Excited State Hydrogen Bonding and Conformational Planarization. *J. Photochem. Photobiol. A* **2023**, *435*, 114210.
(63) Gulyani, A.; Dey, N.; Bhattacharya, S. Tunable Emission from Fluorescent Organic Nanoparticles in Water: Insight into the Nature of Self-Assembly and Photoswitching. *Chem.−Eur. J.* **2018**, *24*, 2643−2652.
(64) Dey, N.; Bhattacharya, S. Switchable Optical Probes for Simultaneous Targeting of Multiple Anions. *Chem.−Asian J.* **2020**, *15*, 1759−1779.
(65) Fernandes, R. S.; Dey, N. Modulation of Analytical Performance of a Bifunctional Optical Probe at the Micelle-Water Interface: Selective Sensing of Histidine in Biological Fluid. *Asian J. Org. Chem.* **2022**, *11*, No. e202200257.
(66) Kathiravan, A.; Sundaravel, K.; Jaccob, M.; Dhinagaran, G.; Rameshkumar, A.; Arul Ananth, D. A.; Sivasudha, T. Pyrene Schiff Base: Photophysics, Aggregation Induced Emission, and Antimicrobial Properties. *J. Phys. Chem. B* **2014**, *118*, 13573−13581.
(67) Rani, B. K.; John, S. A. Pyrene-Antipyrine based Highly Selective and Sensitive Turn-On Fluorescent Sensor for Th(IV). *New J. Chem.* **2017**, *41*, 12131−12138.
(68) Kowser, Z.; Rayhan, U.; Rahman, S.; Georghiou, P. E.; Yamato, T. A Fluorescence "Turn-On" Sensor for Multiple Analytes: OAc^- and F^- Triggered Fluorogenic Detection of Zn^{2+} in a Co-Operative Fashion. *Tetrahedron* **2017**, *73*, 5418−5424.
(69) Correia, B. B.; Brown, T. R.; Reibenspies, J. H.; Lee, H. -S.; Hancock, R. D. Exciplex Formation as an Approach to Selective Copper(II) Fluorescent Sensors. *Inorg. Chim. Acta* **2020**, *506*, 119544.

https://doi.org/10.1021/acsomega.2c06559
ACS Omega 2023, 8, 6349−6360

(70) Singhal, N. K.; Ramanujam, B.; Mariappanadar, V.; Rao, C. P. Carbohydrate-Based Switch-on Molecular Sensor for Cu(II) in Buffer: Absorption and Fluorescence Study of the Selective Recognition of Cu(II) Ions by Galactosyl Derivatives in HEPES Buffer. *Org. Lett.* **2006**, *8*, 3525−3528.
(71) Samanta, S. K.; Dey, N.; Kumari, N.; Biswakarma, D.; Bhattacharya, S. Multimodal Ion Sensing by Structurally Simple Pyridine-End Oligo *p*-Phenylenevinylenes for Sustainable Detection of Toxic Industrial Waste. *ACS Sustainable Chem. Eng.* **2019**, *7*, 12304−12314.
(72) Hosseini, M.; Vaezi, Z.; Ganjali, M. R.; Faridbod, F.; Abkenar, S. D.; Alizadeh, K.; Salavati-Niasari, M. Fluorescence "Turn-On" Chemosensor for the Selective Detection of Zinc Ion based on Schiff-Base Derivative. *Spectrochim. Acta, Part A* **2010**, *75*, 978−982.
(73) Liu, Z. -C.; Yang, Z. -Y.; Li, T. -R.; Wang, B. -D.; Li, Y.; Qin, D. -D.; Wang, M. -F.; Yan, M. -H. An Effective Cu(II) Quenching Fluorescence Sensor in Aqueous Solution and 1D Chain Coordination Polymer Framework. *Dalton Trans.* **2011**, *40*, 9370−9373.
(74) Qin, J. -C.; Yang, Z. -Y. Fluorescent Chemosensor for Detection of Zn^{2+} and Cu^{2+} and Its Application in Molecular Logic Gate. *J. Photochem. Photobiol. A* **2016**, *324*, 152−158.
(75) Biswas, D.; Bar, N.; Pal, S.; Mazumder, S. K.; Ray, A.; Chowdhury, S.; Das, G. K.; Chowdhury, P. Polymer based ON-OFF-ON Fluorescent Logic Gate: Synthesis, Characterization and Understanding. *J. Mol. Struct.* **2022**, *1252*, 132166.
(76) Fernandes, R. S.; Dey, N. Synthetic Supramolecular Host for D-(−)-Ribose: Ratiometric Fluorescence Response via Multivalent Lectin-Carbohydrate Interactions. *ChemBioChem* **2022**, *23*, No. e202200044.
(77) Sachdeva, T.; Milton, M. D. Logic Gate based Novel Phenothiazine-Pyridylhydrazones: Halochromism in Solid and Solution State. *Dyes Pigm.* **2019**, *164*, 305−318.
(78) Pandey, R.; Kumar, A.; Xu, Q.; Pandey, D. S. Zinc(II), Copper(II) and Cadmium(II) Complexes as Fluorescent Chemosensors for Cations. *Dalton Trans.* **2020**, *49*, 542−568.
(79) Dey, N.; Kumari, N.; Biswakarma, D.; Jha, S.; Bhattacharya, S. Colorimetric Indicators for Specific Recognition of Cu^{2+} and Hg^{2+} in Physiological Media: Effect of Variations of Signaling Unit on Optical Response. *Inorg. Chim. Acta* **2019**, *487*, 50−57.
(80) Chakraborty, S.; Lohar, S.; Dhara, K.; Ghosh, R.; Dam, S.; Zangrando, E.; Chattopadhyay, P. A New Half-Condensed Schiff Base Platform: Structures and Sensing of Zn^{2+} and $H_2PO_4^-$ Ions in an Aqueous Medium. *Dalton Trans.* **2020**, *49*, 8991−9001.
(81) Hens, A.; Mondal, P.; Rajak, K. K. Selective $H_2PO_4^-$ Anion Sensing by Two Neutral Zn^{2+} Complexes and Combined Theoretical and Experimental Studies of Their Structural and Spectral Properties. *Polyhedron* **2015**, *85*, 255−266.
(82) Pushina, M.; Farshbaf, S.; Mochida, W.; Kanakubo, M.; Nishiyabu, R.; Kubo, Y.; Anzenbacher, P. A Fluorescence Sensor Array Based on Zinc(II)-Carboxyamidoquinolines: Toward Quantitative Detection of ATP. *Chem.−Eur J.* **2021**, *27*, 11344−11351.
(83) Ojida, A.; Takashima, I.; Kohira, T.; Nonaka, H.; Hamachi, I. Turn-on Fluorescence Sensing of Nucleoside Polyphosphates Using a Xanthene-based Zn(II) Complex Chemosensor. *J. Am. Chem. Soc.* **2008**, *130*, 12095−12101.
(84) Ma, C.; Yang, Y.; Li, C.; Liu, Y. TD-DFT Study of the Double Excited-State Intramolecular Proton Transfer Mechanism of 1,3-Bis(2-pyridylimino)-4,7-dihydroxyisoindole. *J. Phys. Chem. A* **2015**, *119*, 12686−12692.
(85) Yang, Y.; Zhao, J.; Li, Y. Theoretical Study of the ESIPT Process for a New Natural Product Quercetin. *Sci. Rep.* **2016**, *6*, 32152.
(86) Li, G. -Y.; Chu, T. TD-DFT Study on Fluoride-Sensing Mechanism of 2-(2′-phenylureaphenyl)benzoxazole: The Way to Inhibit the ESIPT Process. *Phys. Chem. Chem. Phys.* **2011**, *13*, 20766−20771.

https://doi.org/10.1021/acsomega.2c06559
ACS Omega 2023, 8, 6349−6360